In-flight Measurements of Radiation Environment Observed by Eutelsat 7C (Electric Orbit Raising Satellite)

Pablo Caron, Sébastien Bourdarie, Didier Falguere, Didier Lazaro, Philippe Bourdoux, Vijay Thakur, Pierre Timmerman, Ricardo Hernandez, Grégory Schneider, Catherine Keys, et al.

In-flight Measurements of Radiation Environment Observed by Eutelsat 7C (Electric Orbit Raising Satellite)

P. Caron, S. Bourdarie, D. Falguère, D. Lazaro, P. Bourdoux, V. Thakur, P. Timmerman, R. Hernandez, G. Schneider, C. Keys, M. Baylocq, N. Balcon, D. Standarovski, J. Mekki, R. Ecoffet

***Abstract*—Measurements of particle fluxes (protons and electrons) obtained with the ICARE_NG monitor on the Eutelsat 7C orbit (Electric Orbit Raising to geostationary orbit) are presented. Several comparisons are proposed with other instruments (MagEIS, RPS and MPSH) and radiation models (AEP8, IRENE and GREEN). Significant discrepancies have been found, especially with AEP8 model. The measurements when the satellite is in its operational orbit (GEO) have also been compared with the IGE model and an excellent agreement is observed. For calculating fluxes from ICARE_NG outputs, two methods have been developed and their results are compared in order to consolidate our interpretations.**

***Index Terms*— Space environment, particle fluxes, electron, proton, EOR, GEO.**

I. Introduction

FOR about twenty years, several ICARE (Influence sur les Composants Avancées des Radiations de l'Espace) have been embedded during space missions such as SAC-D [1] and JASON2 [2]. Initially called ICARE, different versions have been released so far to improve the performance of the radiation monitor: ICARE_NG (for New Generation) and now ICARE_NG².

E7C (Eutelsat 7C) is currently the most recent mission on which an ICARE_NG is embedded. The spacecraft was launched by Arianespace, on an Ariane 5 vehicle [3]. It reached its operational orbit (geostationary orbit) by using Electric Orbit Raising (EOR). Several months of measurements of the radiation belts have been performed.

The instrument packages were developed under CNES funding. Ground testing and calibrations were performed at ONERA. The first measurements were acquired on June 21, 2019, at the beginning of the EOR phase. The satellite reached its GEO position about four months later.

Manuscript received November 08, 2021; This work was supported by Grants 4500059441/DIA094, which part of CNES R&T program.

P. Caron, S. Bourdarie, D. Falguère and D. Lazaro are with ONERA/DPHY, Université de Toulouse, Toulouse, France (email: Pablo.Caron@onera.fr)

P. Bourdoux is with the EREMS Society, Flourens, France (email: Philippe.Bourdoux@erems.fr)

V. Thakur, P. Timmerman, R. Hernandez and G. Schneider are with EUTELSAT (email: vthakur@eutelsat.com)

C. Keys and M. Baylocq are with MAXAR (email: Catherine.Keys@maxar.com)

R. Ecoffet, N. Balcon, D. Standarovski and J. Mekki are with CNES, The French Space Agency, Toulouse, France (email: Robert.Ecoffet@cnes.fr)

The radiation monitor is placed inside the satellite and provides electron measurements from 1.5 MeV up to 2.5 MeV and proton measurements from 50 MeV up to 150 MeV.

The first results obtained on-board the E7C satellite are presented and discussed in this paper. First, a description of the monitor and two methods for calculating fluxes are proposed. Then, several comparisons between models, other instruments and ICARE_NG measurements are conducted.

II. Responses of the Radiation Monitor

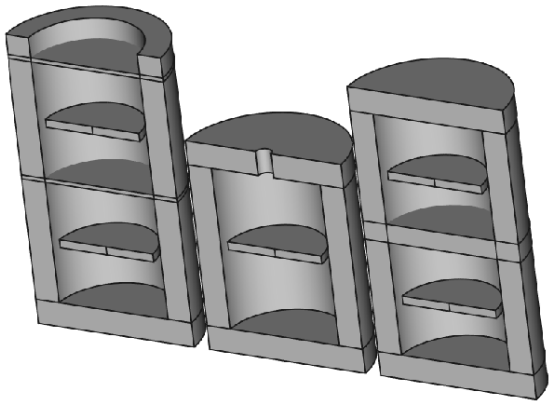

Fig. 1. Schematic view of the three detection heads. From left to right: PE2, PE1 and PE2_S. This arrangement of the detection heads is the one applied on the satellite.

ICARE_NG consists of three detection heads, as presented in Fig. 1:

- One detection head called PE1 for Proton Electron measurements with one diode (silicon detector, 700 µm thick).
- One detection head called PE2 for Proton Electron measurements with two diodes (silicon detectors, 500 µm thick).
- One detection head called PE2_S for Proton Electron measurements with two diodes (silicon detectors, 500 µm thick) and an intermediate Shielding.

In addition, ICARE_NG proposes different acquisition modes:

- Single mode : *the deposited energy sampling is done only on one diode, without considering the other diodes*
- Anticoincidence mode : *the deposited energy sampling is done only on one diode but on the*

condition that there was no interaction with another diode

- Coincidence mode : *the deposited energy sampling is done on one or more diodes as soon as a particle has crossed all the diodes concerned*

As the PE1 head consists of a single diode, only the single mode is available. However, PE2 and PE2_S heads consist of two diodes. Anticoincidence and coincidence modes are then available, associated with different measurement results.
By the way of telecommands, some instrument parameters can be modified such as integration time, the thresholds and the gains. Deposited energies are recorded by the instrument, given as counts distributed over 128 or 256 channels, according to the need of the telemetry rate.

As the radiation monitor is located inside the satellite, the responses to radiative environments of the detection heads can differ from what was initially planned. Indeed, it is necessary to take into account the geometry of the satellite to properly simulate the response functions of each detection heads. Fig. 2 corresponds to Monte-Carlo simulation results of the response function of the PE2 detection head in anticoincidence mode.

Response functions have been performed using GEANT4 (v10.3 patch 01) which is a toolkit for the simulation of the passage of particles through matter [4]–[6]. The geometry of the satellite has been simplified into a sector shielding analysis (ray-tracing). This approach produces distributions of shielding thickness as viewed from the center of the three detection heads as a function of direction from these locations. Incident particles were launched in all directions from any point outside the spacecraft (assuming isotropic fluxes), with different energies. All the deposited energies in the diodes are then recorded. The geometric factor (gef) as plotted in Fig. 2 is calculated according (1) [7].

$$\text{gef} = 4\pi^2 R^2 \frac{N_{det}}{N_{tot}} \quad (1)$$

Where R is the radius of the source of particles, N_{det} is the number of particles that deposit energy in the diode(s) and N_{tot} is the total number of particles launched from the source. As stated in [7], the geometric factor makes the link between the response of the radiation monitor and the radiative environments. The more sensitive the monitor is to a king of particle in a given energy range, the higher the associated geometric factor.

Based on the counts of the instrument and the associated response functions, particle fluxes can then be deduced. Several methods can be applied, using particular shapes of the response functions [1], [2], [8], by solving the Fredholm integral equation of the first kind [9], [10] or using tools from the fields of Artificial Intelligence [11]. Previous works on ICARE and ICARE_NG mainly used the first two methods mentioned and same approaches will also be used in this paper.

Response functions as presented in Fig. 2 contain particular shapes that can be directly used to process the counts of the instrument.

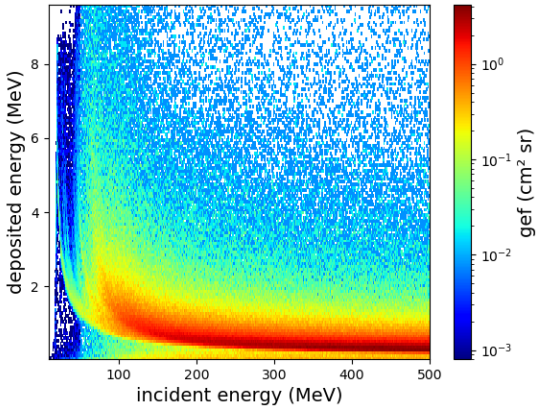

Fig. 2. Proton response function of the PE2 detection head in the anticoincidence mode.

Fig. 3 presents few geometric factors that act as integration operators and thus provide integrated fluxes.

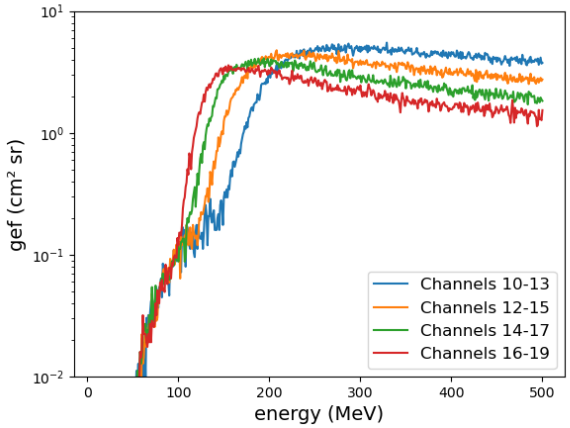

Fig. 3. Proton geometric factors of the PE1 detection head versus incident energy associated with 4 channel groups. Each channel is also associated with a deposited energy.

It is then possible to find the associated parameters (cutoff energy and magnitude in the cases of Fig. 3) by the way of the Bowtie inversion technique [8]. "Virtual fluxes" database has been developed, containing:

- AEP8 fluxes (1 < L < 8 and B=Beq) [12], [13]
- AEP9 fluxes (1 < L < 8 and B=Beq) [14]
- GREEN fluxes (1 < L < 8 and B=Beq) [15]
- Exponential cut-off power law ($f \propto aE^b e^{cE}$), where a, b, c are determined to provide fluxes contained in the envelope of the fluxes from the previous models.

From this database and geometric factors as presented in Fig. 3, it is then possible to evaluate the best parameters (cutoff energy and magnitude for integrated fluxes and mean energy and magnitude for differential fluxes). Table I summarizes the results of this approach for each detection heads and each acquisition modes.

TABLE I
SUMMARIZE OF THE OUTPUTS FROM THE ICARE-NG RADIATION MONITOR ON-BOARD E7C

Head	Mode	Flux type	Proton energies (MeV)	Electron energies (MeV)
PE1	Single	Integral	65 – 115	
PE2	Anticoincidence	Integral	50 – 120	1.5 – 2.5
PE2	Coincidence	Differential	80 – 150	
PE2_S	Anticoincidence	Integral	55 – 100	
PE2_S	Coincidence	Differential	85 - 120	

Proton measurements are then allowed for energies between 50 MeV and 150 MeV while electron measurements are allowed for energies between 1.5 MeV and 2.5 MeV.

As previously mentioned, a second approach has been used. The Fredholm integral equation of the first kind takes the following form [9]:

$$\mathrm{C} = \sum_{n=p,e} \int_0^{\infty} f_{n\,\mathrm{diff}}(E)\mathrm{RF_n}(E)dE \qquad (2)$$

Where $f_{n\,\mathrm{diff}}$ are the electron and proton $(n = p, e)$ differential fluxes and $\mathrm{RF_n}$, are the response functions. This equation is a typical example of an ill-posed problem and its solution is not guaranteed to be unique, nor a continuous function of the counts C.

To solve Eq. (2), several approach are proposed in the literature [9]–[11], [16]. A regularized pseudo-inversion method has been develop to process the E7C data. This leads to the following system:

$$\begin{bmatrix} \mathrm{RF} \\ \sqrt{\lambda}\mathrm{L} \end{bmatrix} \cdot f_{\mathrm{diff}} \cdot \Delta E = \begin{bmatrix} \mathrm{C} \\ 0 \end{bmatrix} \qquad (3)$$

Where λ and L are respectively the regularization parameter and matrix. The L-matrix selected takes the following form:

$$\mathrm{L} = \begin{pmatrix} -1 & 1 & & \\ & -1 & \ddots & 0 \\ & 0 & \ddots & 1 \\ & & & -1 \end{pmatrix} \qquad (4)$$

And the λ parameter was adjusted, depending on the response function used.

Pseudo-inversion (by the way of Singular Value Decomposition) and geometric factor analysis have been applied to the instrument's data (counts) for cross-validation purposes. Typical results of proton fluxes reconstruction are shown in Fig. 4. Inversion method provides continuous fluxes while the deconvolution using groups of channels and associated scalar geometric factors is performed only for some values in energy.

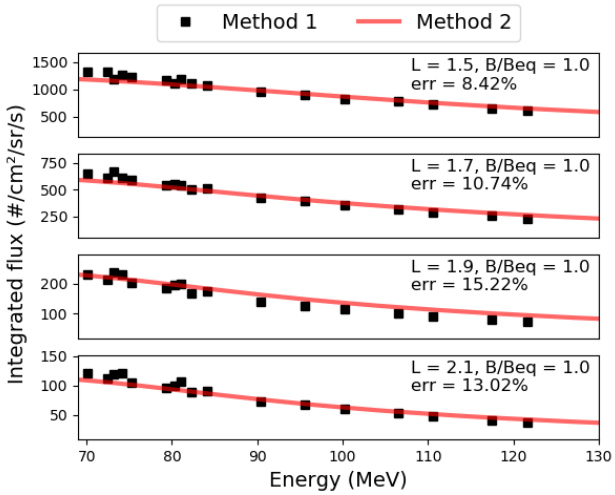

Fig. 4. Counts to proton flux conversion deduced from the two methods presented above. Four cases are considered: L = [1.5, 1.7, 1.9, 2.1] at B/Beq = 1.0. Mean relative errors between each methods are also calculated.

Differential fluxes deduced from inversion method have been integrated to provide "smoothed" curves, which can be directly compared to integrated fluxes deduced with the first method. The overall comparisons between these two methods show very similar results, with an average relative error around 10% on all the compared spectra.

In the following of this paper, data analysis procedure follows the recommendation of the COSPAR Panel for Radiation Belt Environment Modeling (PRBEM) [17].

III. E7C MEASUREMENT COMPARISONS WITH MODELS

Fig. *5* and
Fig. *6* present the evolution of the proton and the electron environments respectively as seen by ICARE_NG aboard E7C during the EOR phase. Low altitudes are covered less and less by the satellite until the operational orbit is reached. Some vertical blank lines can be observed in
Fig. *5* and
Fig. *6* due to data gaps in the telemetries.

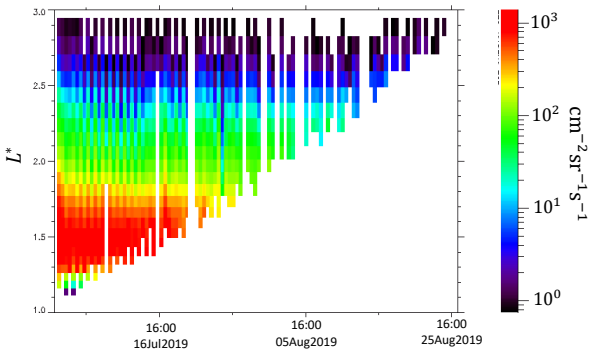

Fig. 5. Evolution of the proton environments (proton fluxes > 94 MeV) plotted thanks to the IPSAT tool *[18]* during the EOR phase which started on June 21.

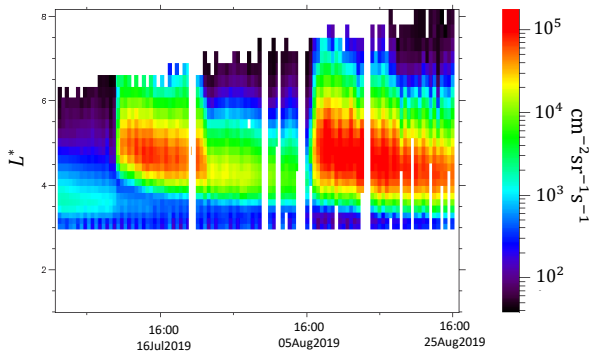

Fig. 6. Evolution of the electron environments (electron fluxes > 1.7 MeV) plotted thanks to the IPSAT tool *[18]* during the EOR phase which started on June 21. A cut is performed for the L* < 3.

To validate all the E7C data collected, several comparisons were conducted. These comparisons concern both electron and proton fluxes.

A. Electron

With an electric propulsion, E7C provides electron data from the radiation belts in addition to the geostationary orbit. Both aspects of the mission are observed here (EOR and GEO).

1) EOR phase

Comparisons with AE8 and AE9 models have been performed (see Fig. 7). The satellite positions filtered in L* and B were injected into the models. The fluxes measured by ICARE_NG were averaged over the entire EOR phase at several L* values, in order to be comparable to the models (which are "average models"). Some of these comparisons are illustrated in Fig. 7.

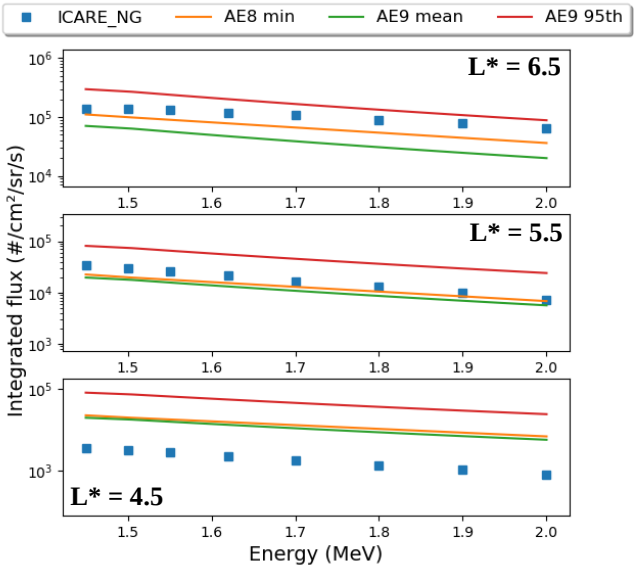

Fig. 7. Electron fluxes measured by ICARE_NG and estimated by AE8 and AE9 models. Three cases are observed: L* = [4.5, 5.5, 6.5].

AE8 and AE9 propose higher fluxes than those observed by ICARE_NG for L* lower than ~ 5. This suggests that the models are overestimating these fluxes for two reasons:

- For higher L*, the ICARE_NG data are within the envelope proposed by the models
- If the ICARE_NG data were contaminated by other particles or electronic noise, the conclusion would be reversed and the fluxes should be higher than those of the models

Thus, for L* higher than ~ 5, good agreement can be observed between the measurements and the models, especially the AE8 min model.

2) GEO

Comparisons with AE8 [12], AE9 [14] and IGE [15], [19] radiation models have been performed, as presented in Fig. 8. As IGE model is dedicated to geostationary orbit, only ICARE_NG data when E7C is on station are analyzed.

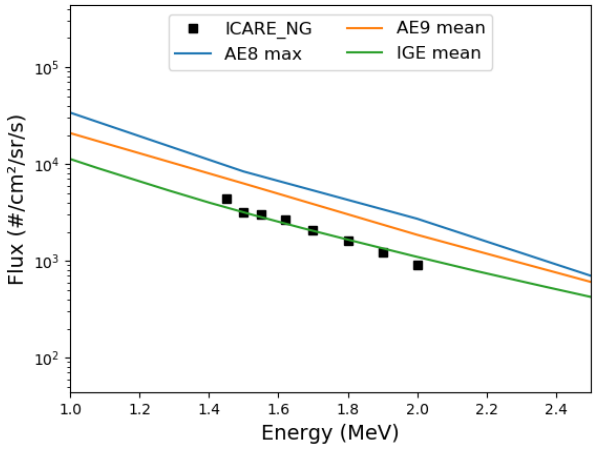

Fig. 8. AE8, AE9, IGE and ICARE_NG comparisons in GEO.

Several months (from November 2019 to March 2020) of measurements were averaged to obtain the results presented in Fig. 8. Unlike AE8 model, IGE model (which is integrated in GREEN-e model [15], [20]) takes into account the solar cycle variation. It was therefore expected that this model would be more consistent with our data. And indeed, as can be seen in Fig. 8, the ICARE_NG data are in excellent agreement with the IGE model. However, AE8 max and AE9 mean provide higher results than the ICARE_NG measurements, by a factor of 2 or 3.

B. Proton

As for the electrons, a comparative study of the proton fluxes measured by ICARE_NG has been performed with the AP8 and AP9 models. Fig. 9 illustrates our findings during the EOR phase. No comparison in GEO orbit will be proposed because, at this altitude, the proton population is too low at the energies measured by ICARE_NG.

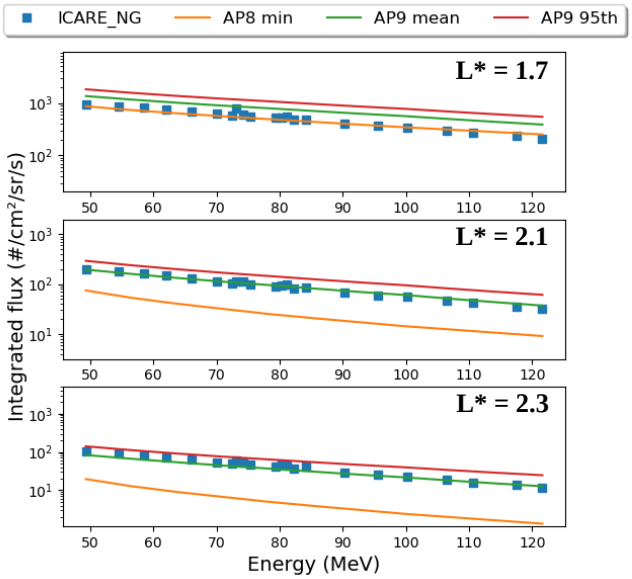

Fig. 9. Proton fluxes measured by ICARE_NG and estimated by AP8 and AP9 models. Three cases are observed: L* = [1.7, 2.1, 2.3].

Significant differences can be observed between the fluxes measured by ICARE_NG and the fluxes estimated by the AP8 model. These differences are mainly significants for the last case but is observed more and more as we go up in altitude. Indeed, the lower L* value is, the more the ICARE_NG measurements and the AP8 model agree. In contrast, AP9 offers higher fluxes than ICARE_NG at low L* values but is better matched at high L* values. For L* higher than ~ 2, the ICARE_NG measurements are included in the envelope deduced from the AP9 mean and 95th models (see Fig. 9 for L* = 2.1 and 2.3).

IV. E7C Measurement Comparisons with Other In-Flight Measurements

A. *Electron*

Comparisons with the MPSH instruments (Magnetospheric Particle Sensors High) [21] aboard the GOES-16 spacecraft (Geostationary Operational Environmental Satellite) have been performed, as presented in Fig. 10. This instrument measures protons in the 50 keV to 12 MeV energy range (which is outside the energies targeted by ICARE_NG) and electrons in the 50 keV to 4 MeV energy range. As ICARE_NG, MPSH is an SSD-based monitor.

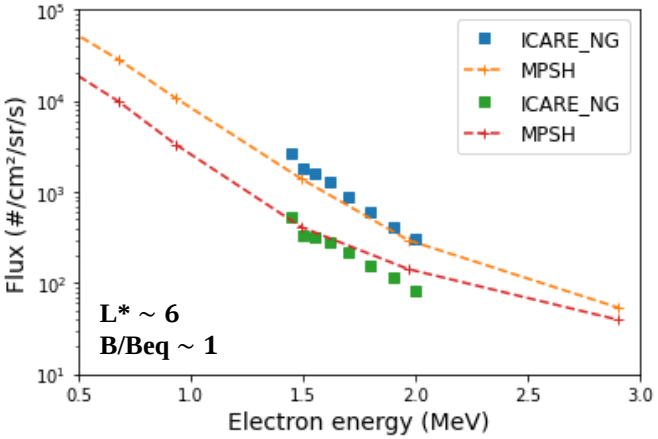

Fig. 10. Comparisons of ICARE_NG aboard E7C measurements and MPSH aboard GOES-16 measurements. Two magnetic conjunctions are proposed.

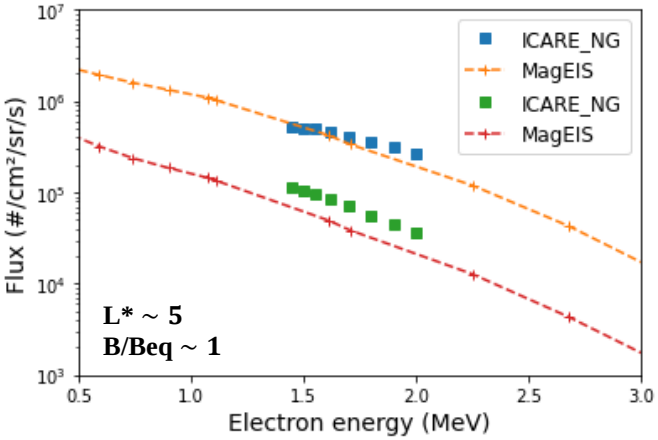

Fig. 11. Comparisons of ICARE_NG aboard E7C measurements and MagEIS aboard RBSP measurements. Two magnetic conjunctions are proposed.

To properly compare the measurements of the two instruments, magnetic conjunctions were looked for. Such conjunctions allow to filter the positions of satellites in comparable magnetic regions by constraining three important parameters:

- the Roederer L* parameter [22]
- B/Beq, the magnetic field and equatorial magnetic field ratio
- the magnetic local time MLT

Between two satellites, up to 5% error was accepted on each of these parameters and some magnetic conjunctions could thus be found. Two magnetic conjunctions are proposed in Fig. 10 where the L* values are close to 6 and B/Beq close to 1. In both cases, very similar fluxes (in terms of intensities and dynamics) can be noticed. Such agreement between two different instruments strengthens the validity of the measurements.

Equivalent analysis has been performed with the MagEIS instruments (Magnetic Electron Ion Spectrometer) aboard the RBSP spacecraft (Radiation Belt Storm Probes) [23]. Some magnetic conjunctions (L* near to 5 and B/Beq near to 1) have been found during the EOR phase of E7C. Fig. 11 presents two cases.

Both instruments provide relatively similar measurements, although ICARE_NG measurements seem to produce slightly higher electron fluxes than MagEIS in some cases (on average

on the few magnetic conjunctions found, the relative error between these two instruments is less than 30%).

B. Proton

Comparisons with proton flux measurements from RPS (Relativistic Proton Spectrometer) aboard RBSP_B (Radiation Belt Storm Probes) [24] have been performed. Fig. 12 presents the case of 105 MeV protons. An important point is that both instruments operated at the same time.

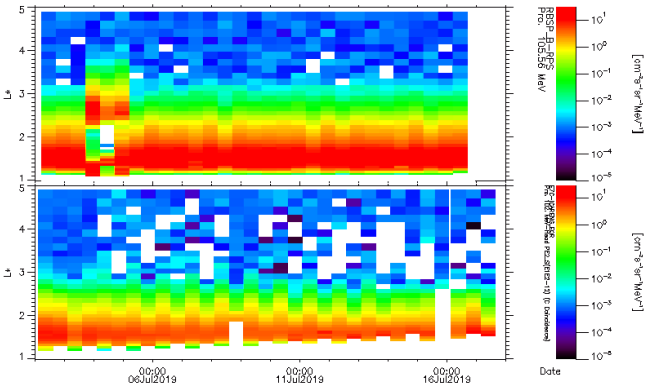

Fig. 12. Evolution of 105 MeV proton fluxes observed by RPS (top) and ICARE_NG (bottom) as a function of time and L*.

There are substantial differences between the measurements of RPS and ICARE_NG. In particular, ICARE_NG provides lower fluxes than those measured by RPS (by a factor of about 2 in the heart of the inner belt). However, the size of the proton belt is quite close from one instrument to another.

V. Conclusion

The ICARE_NG radiation monitor aboard Eutelsat 7C has been presented. Electron measurements from 1.5 MeV up to 2.5 MeV and proton measurements from 50 MeV up to 150 MeV are provided both during the EOR phase and the operational orbit (GEO).

Two methods for converting instrument observations (counts) to particle fluxes have been presented and discussed. Their respective performances have also been presented through the paper.

Many comparisons have been performed, with measurements from other instruments and with estimations from models (AEP8, AEP9 and IGE). Concerning the electron data:

- Significant differences have been highlighted between AE8min, AE9mean and ICARE_NG measurements for L* values lower than ~ 5. This is even more pronounced with the 95th percentile of AE9.
- At geostationary orbit, IGE describes very well the electron fluxes.
- MPSH, MagEIS and ICARE_NG instruments provide quite similar electron fluxes (according to the few conjunctions found, ICARE_NG and MPSH have an average relative deviation of less than 20% while MagEIS and ICARE_NG have an average relative deviation of less than 30%).

Concerning proton fluxes:

- For L* values greater than ~ 2, important variations have been observed between the AP8min model and the ICARE_NG measurements while AP9 (mean and 95th) are more consistent with the measured fluxes.
- There is a factor of ~ 2 between ICARE_NG and RPS measurements in the heart of the inner belt.

Acknowledgment

Processing and analysis of the MagEIS data was supported by Energetic Particle, Composition, and Thermal Plasma (RBSP-ECT) investigation funded under NASA's Prime contract no. NAS5-01072. All RBSP-ECT data are publicly available at the Web site http://www.RBSP-ect.lanl.gov/.

The authors would like to thank Eutelsat and Maxar for Eutelsat 7C data provision.

References

[1] D. Boscher *et al.*, "In-Flight Measurements of Radiation Environment on Board the Argentinean Satellite SAC-D," *IEEE Trans. Nucl. Sci.*, vol. 61, no. 6, pp. 3395–3400, Dec. 2014, doi: 10.1109/TNS.2014.2365212.

[2] D. Boscher *et al.*, "In Flight Measurements of Radiation Environment on Board the French Satellite JASON-2," *IEEE Trans. Nucl. Sci.*, vol. 58, no. 3, pp. 916–922, Jun. 2011, doi: 10.1109/TNS.2011.2106513.

[3] Arianegroup, "Flight VA248: Arianespace will orbit T-16 and Eutelsat-7c for two world-class satellite operators." [Online]. Available: https://www.arianespace.com/wp-content/uploads/2019/06/VA248-launch-kit_EN.pdf

[4] S. Agostinelli *et al.*, "Geant4—a simulation toolkit," *Nucl. Instrum. Methods Phys. Res. Sect. Accel. Spectrometers Detect. Assoc. Equip.*, vol. 506, no. 3, pp. 250–303, Jul. 2003, doi: 10.1016/S0168-9002(03)01368-8.

[5] J. Allison *et al.*, "Geant4 developments and applications," *IEEE Trans. Nucl. Sci.*, vol. 53, no. 1, pp. 270–278, Feb. 2006, doi: 10.1109/TNS.2006.869826.

[6] J. Allison *et al.*, "Recent developments in Geant4," *Nucl. Instrum. Methods Phys. Res. Sect. Accel. Spectrometers Detect. Assoc. Equip.*, vol. 835, pp. 186–225, Nov. 2016, doi: 10.1016/j.nima.2016.06.125.

[7] J. D. Sullivan, "Geometric factor and directional response of single and multi-element particle telescopes," *Nucl. Instrum. Methods*, vol. 95, no. 1, pp. 5–11, Aug. 1971, doi: 10.1016/0029-554X(71)90033-4.

[8] A. Boudouridis, J. V. Rodriguez, B. T. Kress, B. K. Dichter, and T. G. Onsager, "Development of a Bowtie Inversion Technique for Real-Time Processing of the GOES-16/-17 SEISS MPS-HI Electron Channels," *Space Weather*, vol. 18, no. 4, Art. No. e2019SW002403, Apr. 2020, doi: 10.1029/2019SW002403.

[9] I. Sandberg, I. A. Daglis, A. Anastasiadis, P. Bühler, P. Nieminen, and H. Evans, "Unfolding and validation of SREM fluxes," in *2011 12th European Conference on Radiation and Its Effects on Components and Systems*, Sep. 2011, pp. 599–606. doi: 10.1109/RADECS.2011.6131429.

[10] V. Maget *et al.*, "Unfolding JASON-2/ICARE-NG high energy particles measurements using a Singular Value

Decomposition approach," in *2013 14th European Conference on Radiation and Its Effects on Components and Systems (RADECS)*, Oxford, United Kingdom, Sep. 2013, pp. 1–7. doi: 10.1109/RADECS.2013.6937422.

[11] S. Aminalragia-Giamini *et al.*, "Artificial intelligence unfolding for space radiation monitor data," *J. Space Weather Space Clim.*, vol. 8, p. A50, 2018, doi: 10.1051/swsc/2018041.

[12] J. I. Vette, *The AE-8 Trapped Electron Model Environment*. National Space Science Data Center (NSSDC), World Data Center A for Rockets and Satellites (WDC-A-R&S), National Aeronautics and Space Administration, Goddard Space Flight Center, 1991.

[13] D. M. Sawyer and J. I. Vette, *AP-8 trapped proton environment for solar maximum and solar minimum*. National Space Science Data Center (NSSDC), World Data Center A for Rockets and Satellites (WDC-A-R&S), 1976.

[14] G. P. Ginet *et al.*, "AE9, AP9 and SPM: New Models for Specifying the Trapped Energetic Particle and Space Plasma Environment," in *The Van Allen Probes Mission*, N. Fox and J. L. Burch, Eds. Boston, MA: Springer US, 2014, pp. 579–615. doi: 10.1007/978-1-4899-7433-4_18.

[15] A. Sicard, D. Boscher, S. Bourdarie, D. Lazaro, D. Standarovski, and R. Ecoffet, "GREEN: A new Global Radiation Earth ENvironment model," Magnetosphere & space plasma physics/Radiation belts, preprint, Mar. 2018. doi: 10.5194/angeo-2018-26.

[16] J. Půlpán and M. Králík, "The unfolding of neutron spectra based on the singular value decomposition of the response matrix," *Nucl. Instrum. Methods Phys. Res. Sect. Accel. Spectrometers Detect. Assoc. Equip.*, vol. 325, no. 1–2, pp. 314–318, Feb. 1993, doi: 10.1016/0168-9002(93)91032-I.

[17] S. Bourdarie *et al.*, "Data analysis procedure." [Online]. Available: https://prbem.github.io/documents/Standard_Data_Analysis.pdf

[18] S. Bourdarie *et al.*, "IPSAT: Ionizing particle in space analysis tool," *Acta Astronaut.*, vol. 63, no. 1, pp. 471–474, Jul. 2008, doi: 10.1016/j.actaastro.2007.12.033.

[19] A. Sicard-Piet *et al.*, "A new international geostationary electron model: IGE-2006, from 1 keV to 5.2 MeV: GEOSTATIONARY ELECTRON MODEL," *Space Weather*, vol. 6, no. 7, S07003, Jul. 2008, doi: 10.1029/2007SW000368.

[20] A. Sicard, D. Boscher, D. Lazaro, S. Bourdarie, D. Standarovski, and R. Ecoffet, "New Model for the Plasma Electrons Fluxes (Part of GREEN Model)," *IEEE Trans. Nucl. Sci.*, vol. 66, no. 7, pp. 1738–1745, Jul. 2019, doi: 10.1109/TNS.2019.2923005.

[21] G. E. Galica, B. K. Dichter, S. Tsui, M. J. Golightly, C. Lopate, and J. J. Connell, "GOES-R Space Environment In-Situ Suite: instruments overview, calibration results, and data processing algorithms, and expected on-orbit performance," New Delhi, India, May 2016, p. 988118. doi: 10.1117/12.2228537.

[22] J. G. Roederer and S. Lejosne, "Coordinates for Representing Radiation Belt Particle Flux," *J. Geophys. Res. Space Phys.*, vol. 123, no. 2, pp. 1381–1387, Feb. 2018, doi: 10.1002/2017JA025053.

[23] J. B. Blake *et al.*, "The Magnetic Electron Ion Spectrometer (MagEIS) Instruments Aboard the Radiation Belt Storm Probes (RBSP) Spacecraft," *Space Sci. Rev.*, vol. 179, no. 1–4, pp. 383–421, Nov. 2013, doi: 10.1007/s11214-013-9991-8.

[24] J. Mazur *et al.*, "The Relativistic Proton Spectrometer (RPS) for the Radiation Belt Storm Probes Mission," *Space Sci. Rev.*, vol. 179, no. 1–4, pp. 221–261, Nov. 2013, doi: 10.1007/s11214-012-9926-9.